A parametric study for the generation of ion Bernstein modes from a discrete spectrum to a continuous one in the inner magnetosphere. II. Particle-in-cell simulations

Jicheng Sun, Xinliang Gao, Quanming Lu, Lunjin Chen, Xin Tao, and Shui Wang

Citation: Physics of Plasmas **23**, 022902 (2016); doi: 10.1063/1.4941284
View online: http://dx.doi.org/10.1063/1.4941284
View Table of Contents: http://scitation.aip.org/content/aip/journal/pop/23/2?ver=pdfcov
Published by the AIP Publishing

A parametric study for the generation of ion Bernstein modes from a discrete spectrum to a continuous one in the inner magnetosphere. II. Particle-in-cell simulations

Jicheng Sun,[1,2] Xinliang Gao,[1,2,a)] Quanming Lu,[1,2] Lunjin Chen,[3] Xin Tao,[1,2] and Shui Wang[1,2]
[1]CAS Key Laboratory of Geospace Environment, Department of Geophysics and Planetary Science, University of Science and Technology of China, Hefei 230026, China
[2]Collaborative Innovation Center of Astronautical Science and Technology, Harbin 150001, China
[3]Department of Physics, University of Texas at Dallas, Richardson, Texas 75080-3021, USA

(Received 9 November 2015; accepted 30 December 2015; published online 10 February 2016)

In this paper, we perform one-dimensional particle-in-cell simulations to investigate the properties of perpendicular magnetosonic waves in a plasma system consisting of three components: cool electrons, cool protons, and tenuous ring distribution protons, where the waves are excited by the tenuous proton ring distribution. Consistent with the linear theory, the spectra of excited magnetosonic waves can change from discrete to continuous due to the overlapping of adjacent unstable wave modes. The increase of the proton to electron mass ratio, the ratio of the light speed to the Alfven speed, or the concentration of protons with a ring distribution tends to result in a continuous spectrum of magnetosonic waves, while the increase of the ring velocity of the tenuous proton ring distribution leads to a broader one, but with a discrete structure. Moreover, the energization of both cool electrons and protons and the scattering of ring distribution protons due to the excited magnetosonic waves are also observed in our simulations, which cannot be predicted by the linear theory. Besides, a thermalized proton ring distribution may lead to the further excitation of several lower discrete harmonics with their frequencies about several proton gyrofrequencies. © *2016 AIP Publishing LLC*.
[http://dx.doi.org/10.1063/1.4941284]

I. INTRODUCTION

Ion Bernstein modes in the magnetosphere, also known as equatorial noises or magnetosonic waves, which propagate nearly perpendicular to the background magnetic field, are frequently observed in the vicinity of the geomagnetic equator in the region between L = 2 and 8.[1–5] In Paper I by Sun *et al.*,[6] we have examined the linear properties of perpendicular magnetosonic waves excited by a tenuous proton ring distribution under different plasma conditions. The frequencies of magnetosonic waves range from the proton gyrofrequency to the lower hybrid frequency. With the increase of the proton to electron mass ratio and the ratio of the light speed to the Alfven speed, the spectrum of magnetosonic waves becomes broader and continuous from only several discrete modes. Such a continuous spectrum is formed due to the merging of growth rate peaks. The increase in the concentration of protons of the ring distribution can enhance the growth rate of the excited waves, which may also change the spectrum from a discrete to a continuous form, while the increase of the ring velocity of the tenuous proton ring distribution tends to cause a broader but discrete spectrum.

In this paper, with a one-dimensional (1D) particle-in-cell (PIC) simulation model, we investigate the linear and nonlinear properties of perpendicular magnetosonic waves excited by a tenuous proton ring distribution. The linear properties of these waves under different plasma conditions are reproduced in our PIC simulations, and the effects of magnetosonic waves on cool electrons, cool protons, and ring distribution protons are also studied.

The paper is organized as follows. Sec. II describes the simulation model. The simulation results are presented in Sec. III. At last, conclusions and discussion are given in Sec. IV.

II. SIMULATION MODEL

In this paper, 1D electromagnetic PIC simulations are employed to investigate the excitation of magnetosonic waves driven by a proton ring distribution. The 1D PIC simulations allow spatial variations only in the x direction, and periodic boundary conditions are used. The uniform background magnetic field $\mathbf{B}_0$ is along the y axis. It is reasonable to study the evolution of the magnetosonic waves with 1D PIC simulations, since magnetosonic waves usually propagate perpendicular to the background magnetic field.[2–7]

Initially, we assume a uniform and magnetized plasma consisting of three components: cool electrons, cool protons, and ring distribution protons. Their number densities are n_e, n_{hc}, and n_{hr}, respectively. To satisfy the charge neutrality, it requires $n_e = n_{hc} + n_{hr}$. The distribution function of ring distribution protons is given by $f_{hr} = n_{hr}\delta(v_{||})\delta(v_\perp - V_R)/(2\pi v_\perp)$, where $v_{||}$ and $v_\perp$ are velocities parallel and perpendicular to the background magnetic field $\mathbf{B}_0 = B_0\mathbf{e}_y$, and V_R is the proton ring velocity. If not mentioned explicitly, the proton ring velocity is set $V_R = 1.0V_A$, where V_A is the Alfven speed. The cool electrons and cool protons are assumed to satisfy a

a)Author to whom correspondence should be addressed. Electronic mail: gaoxl@mail.ustc.edu.cn

Maxwellian distribution. The thermal speed of the cool protons is set to $0.00635V_A$ and the corresponding $\beta_p = 4 \times 10^{-5}$.The cool electrons adopt the same temperature as cool protons.

In the simulations, the number densities are normalized to the electron number density n_e, and the velocities are expressed in the units of the Alfven speed V_A. Space and time are expressed in the units of the proton inertial length $\lambda_i = \sqrt{m_h/n_e\mu_0 e^2}$ and the inverse of the proton cyclotron frequency $\Omega_h = eB_0/m_h$, respectively, where m_h is proton mass, μ_0 is vacuum permeability, and e is elementary charge. The number of grid cells is 8192, and there are on average 60 macroparticles in every cell for each species. The grid cell size and time step are $\Delta x = 10^{-3}V_A/\Omega_h$ and $\Delta t = 0.5 \times 10^{-4}{\Omega_h}^{-1}$ when the light speed is chosen as $c/V_A = 12$, while $\Delta x = 0.75 \times 10^{-3}V_A/\Omega_h$ and $\Delta t = 0.25 \times 10^{-4}{\Omega_h}^{-1}$ when $c/V_A = 20$.

III. SIMULATION RESULTS

The linear theory has predicted that the proton ring distribution can excite magnetosonic waves propagating perpendicular to the background magnetic field.[7] At the same time, with the increase of proton-to-electron mass ratio, the ratio of the light speed to the Alfven speed, or the concentration of ring distribution protons, the linear growth rate (normalized by the proton cyclotron frequency) of generated waves increases. As a result, the spectrum of magnetosonic waves can change from discrete to continuous. The detailed theoretical results have already been elaborated in Paper I.[6] In this paper, we use 1D PIC simulations to study the excitation of magnetosonic waves by a proton ring distribution and compare the result with that obtained from the linear theory. The parameters for different PIC simulations are listed in Table I. For clarity, the maximum growth rates obtained from both simulations $\gamma(k_{max})/\Omega_h$ and the linear theory[6] $\gamma^*(k_{max})/\Omega_h$, and the saturation amplitudes $(\delta B^2/B_0^2)_{\max}$ have also been listed in Table I. To calculate the maximum growth rates, we first obtain the time profile of wave amplitudes for the wave number with the largest growth rate predicted by the linear theory, and then calculate its slope before the saturation stage as the maximum growth rate. The saturation amplitude is determined by the maximum amplitude during the simulation.

TABLE I. Parameters for different simulation cases.

Case	$\frac{V_R}{V_A}$	$\frac{n_{hr}}{n_e}$	$\frac{c}{V_A}$	$\frac{m_h}{m_e}$	$\frac{\gamma^*(k_{max})}{\Omega_h}$[a]	$\frac{\gamma(k_{max})}{\Omega_h}$	$\left(\frac{\delta B^2}{B_0^2}\right)_{\max}$
1	1	2.0%	12	100	0.29 (9.2)[b]	0.20	1.95×10^{-3}
2	1	2.0%	20	1600	0.73 (15.7)	0.60	1.52×10^{-3}
3	1	2.0%	20	100	0.33 (8.9)	0.32	1.66×10^{-3}
4	1	2.0%	20	900	0.69 (14.6)	0.56	1.37×10^{-3}
5	1	2.0%	12	1600	0.35 (11.3)	0.27	1.92×10^{-3}
6	1	0.5%	20	1600	0.36 (15.7)	0.30	0.40×10^{-3}
7	1	1.0%	20	1600	0.49 (15.4)	0.48	0.60×10^{-3}
8	1.3	1.0%	20	1600	0.34 (15.4)	0.31	1.17×10^{-3}

[a]The k_{max} is the wave number with the maximum growth rate based on the linear theory.

[b]The value out of the parenthesis is the maximum growth rate, while the value within it is the corresponding wave number k_{max}. The unit of wave numbers is Ω_h/V_A.

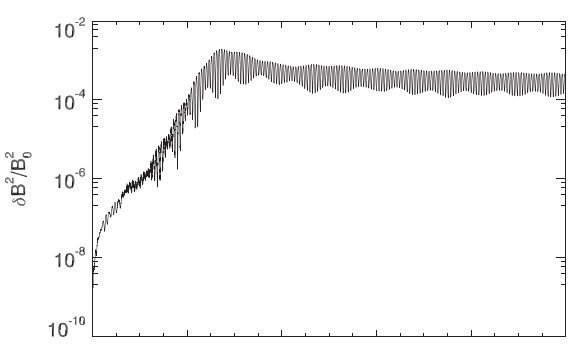

FIG. 1. Time evolution of spatially averaged wave energy for fluctuating magnetic fields $\delta B^2/\delta B_0^2$ for case 1.

Figure 1 shows the time evolution of spatially averaged fluctuating magnetic fields for case 1. The intensities of $\delta B_x/B_0$ and $\delta B_z/B_0$ are below the noise level, and the magnetic field $\delta B/B_0 \approx \delta B_y/B_0$. The magnetosonic waves begin to be excited at about $\Omega_h t = 20$, and then undergo a linear growth stage. A saturation stage is reached at about $\Omega_h t = 40$. The power spectrum, which is obtained by Fourier transforming of $\delta B_y/B_0$ from $\Omega_h t = 0$ to 60, is displayed in Fig. 2. The discrete peaks at harmonic frequencies $\omega = 5\Omega_h$, $6\Omega_h$, and $7\Omega_h$ are clearly observed. These discrete spectral peaks are consistent with the growth rate profile predicted from the linear theory[6] (red lines in Fig. 2).

Figures 3(a) and 3(b) show the fluctuating magnetic field $\delta B_y/B_0$ as a function of wave numbers at $\Omega_h t = 25$ and 80, respectively. At the linear growth stage ($\Omega_h t = 25$), the energy of fluctuating magnetic fields concentrates at $kV_A/\Omega_h \approx 9$. While at the saturation stage ($\Omega_h t = 80$), the peak at $kV_A/\Omega_h \approx 9$ is reduced and the energy of fluctuating magnetic field spreads into a broader wavenumber space.

We also investigate the evolution of velocity distributions for cool electrons, cool protons, and energetic ring distribution protons during the excitation of magnetosonic waves. Figures 4(a) and 4(b) show the electron velocity distribution for case

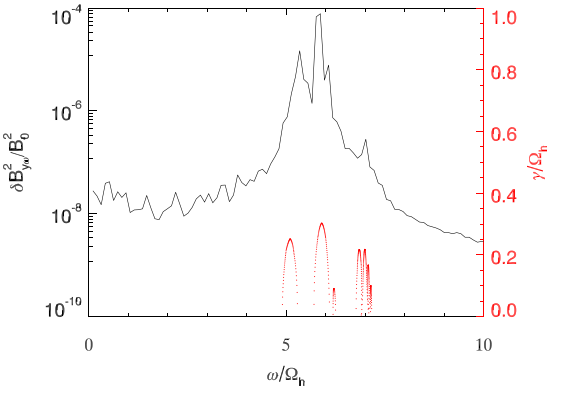

FIG. 2. The power spectrum obtained by Fourier transforming of $\delta B_y/B_0$ from $\Omega_h t = 0$ to 60 for case 1, which is shown by the black line. The red line in the panel denotes the growth rate γ/Ω_h calculated by the linear theory with the same parameters.

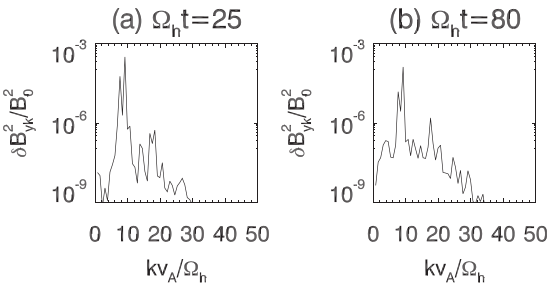

FIG. 3. The fluctuating magnetic field $\delta B_y/B_0$ as a function of wave numbers for case 1 at (a) $\Omega_h t = 25$ and (b) $\Omega_h t = 80$.

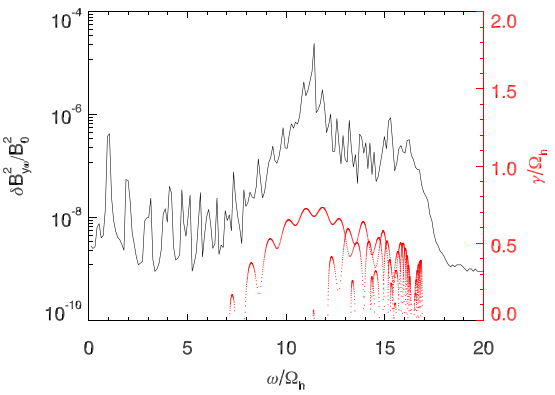

FIG. 5. The power spectrum obtained by Fourier transforming of $\delta B_y/B_0$ from $\Omega_h t = 0$ to 60 for case 2, which is shown by the black line. The red line in the panel denotes the growth rate γ/Ω_h calculated by the linear theory with the same parameters.

1 at $\Omega_h t = 0$ and 80, and Figure 4(c) displays the time profile of electron kinetic energy, Figures 4(d)–4(f) for ring distribution protons, and Figures 4(g)–4(i) for cool protons. In first two columns, solid and dashed lines denote the total and parallel velocity distributions, respectively. It is worth noting that for ring distribution protons, only perpendicular kinetic energy is shown in Fig. 4(f) due to their negligible parallel kinetic energy. For the same reason, we only plot their total velocity distribution in Figs. 4(d) and 4(e). Initially, the electron velocity distribution satisfies a Maxwellian distribution. At the saturation stage ($\Omega_h t = 80$), the electron velocity distribution becomes broader which indicates the increase of the temperature (Fig. 4(b)). As shown in Fig. 4(c), the heating of electrons by the excited magnetosonic waves mainly occurs in the perpendicular direction. The perpendicular energization of cool protons due to the excited magnetosonic waves can also be found in the bottom row. However, for ring distribution protons shown in the middle row, their velocity distribution is scattered into a thick shell distribution, and they lose a part of kinetic energy to generate the magnetosonic waves. For all three components, their parallel velocity distributions nearly remain unchanged, which are consistent with the negligible increase in parallel kinetic energies as shown in the third column. It is shown that the temporal evolution of the perpendicular kinetic energies of cool protons and electrons is closely correlated with that of wave amplitudes (Figure 1). This is because cool protons and electrons are the carrier of excited waves, and their velocities are coupled with the wave electromagnetic fields. However, the perpendicular spread of the proton ring distribution is due to the phase trapping by the excited waves,[7] which then contributes to the saturation of the instability. The involved particle dynamics are interesting and

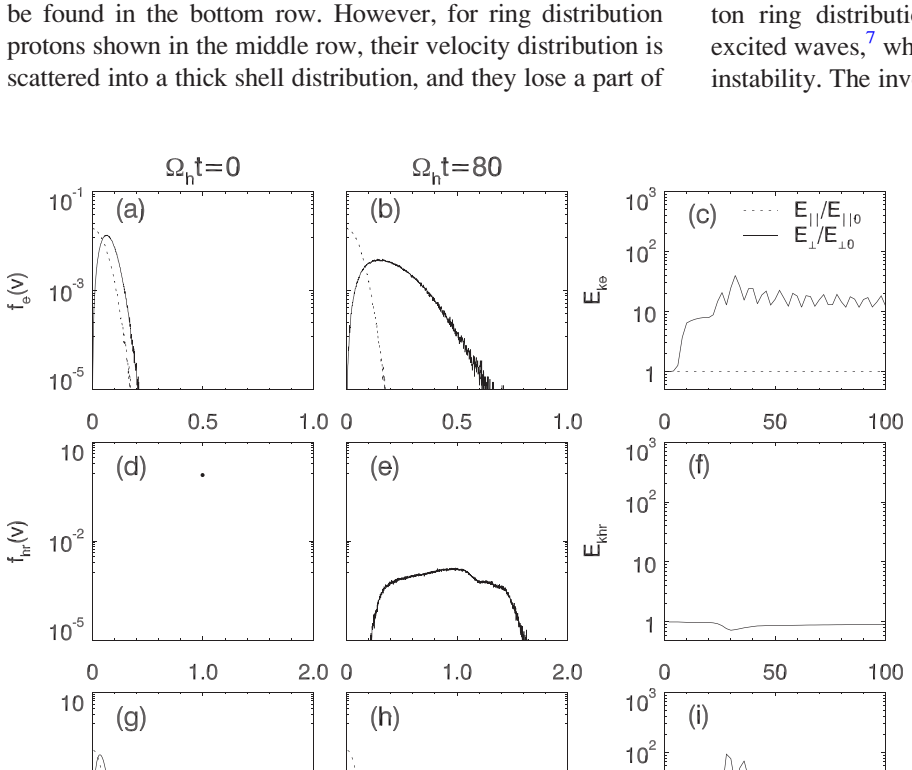

FIG. 4. The electron velocity distributions for case 1 at (a) $\Omega_h t = 0$ and (b) $\Omega_h t = 80$, and (c) the time profile of electron kinetic energy, while (d)–(f) for cool protons, and (g)–(i) for ring distribution protons. In first two columns, solid and dashed lines denote the total and parallel velocity distributions, respectively. The solid and dotted lines in the third column denote perpendicular and parallel kinetic energy, respectively.

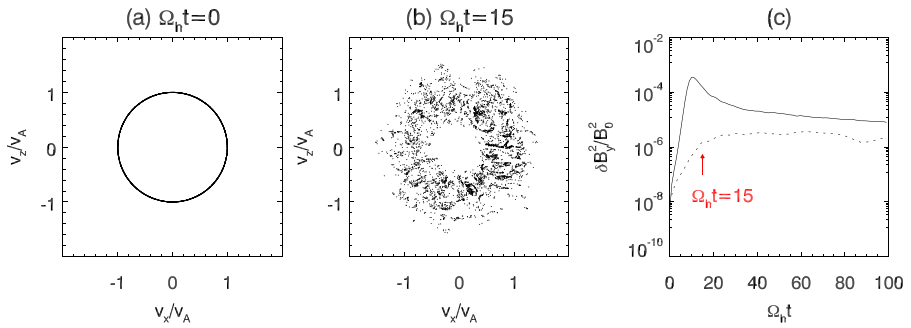

FIG. 6. Scatter plots of ring protons in the (v_x, v_z) space for case 2 at (a) $\Omega_h t = 0$ and (b) $\Omega_h t = 30$, and (c) the time evolution of magnetic amplitudes for lower (1–6 Ω_h, dotted line) and higher (7–17 Ω_h, solid line) harmonic modes.

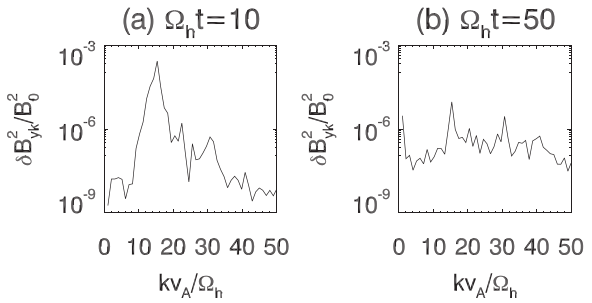

FIG. 7. The fluctuating magnetic field $\delta B_y/B_0$ as a function of wave numbers for case 2 at (a) $\Omega_h t = 25$ and (b) $\Omega_h t = 80$.

need to be further studied, but it is beyond the scope of this paper.

For case 2, the time profile of fluctuating magnetic fields is quite similar to that for case 1, but with a much larger growth rate (Table I). Figure 5 displays the power spectrum, which is obtained by Fourier transforming of $\delta B_y/B_0$ from $\Omega_h t = 0$ to 60 for case 2. The spectral power density shows a continuous structure with a peak near $\omega = 11.5\Omega_h$. The continuous spectrum extends from about $\omega = 9\Omega_h$ to $15\Omega_h$, which is in agreement with the result obtained from the linear theory (red lines in Fig. 6). However, the spectrum also shows discrete peaks at harmonic frequencies 1, 2, …, and $6\Omega_h$, which are not predicted by the linear theory (red lines in Fig. 5). The generation of these harmonic modes can be explained based on Fig. 6, which shows scatter plots of the ring distribution protons in the spatial region from $x = 3$ to 3.05 V_A/Ω_h at (a) $\Omega_h t = 0$ and (b) $\Omega_h t = 15$, and (c) the time evolution of magnetic amplitudes for lower (1–6 Ω_h, dotted line) and higher (7–17 Ω_h, solid line) harmonic modes. To obtain the time evolution of wave amplitudes, we first decompose the time series of $\delta B_y/B_0$ with the wavelet method to get the wave power as functions of time and frequency. Then, the magnetic amplitudes are calculated through the integration of wave power from 1 Ω_h to 6 Ω_h and 7 Ω_h to 17 Ω_h at each time. We can find that the ring distribution protons will be scattered by the magnetosonic waves when the waves are excited. There are many protons with velocities exceeding the Alfven speed. Based on the linear theory, as proton ring velocity increases, the instability shifts toward lower harmonics.[8] Those protons with velocities exceeding the Alfven speed might be responsible for generating the magnetosonic waves with frequencies 1, 2, …, and $6\Omega_h$. This can also be confirmed by the continuous increase in wave amplitudes of lower harmonic modes as found in Fig. 6(c), even after the saturation of higher harmonic modes.

Figures 7(a) and 7(b) display the fluctuating magnetic field $\delta B_y/B_0$ as a function of wave numbers for case 2 at $\Omega_h t = 10$ and 50, respectively. At the linear growth stage ($\Omega_h t = 10$), the energy of fluctuating magnetic field concentrates at $kV_A/\Omega_h \approx 15$. At the saturation stage ($\Omega_h t = 50$), the energy of fluctuating magnetic field also extends into a broader wavenumber space. Similar to case 1, the energization of each component is dominant in the perpendicular direction (not shown).

Figure 8(a) presents the energy of fluctuating magnetic field $\delta B^2/B_0^2$ versus the normalized wave frequency ω/Ω_h for case 3, Figure 8(b) for case 4, and Figure 8(c) for case 2. With the increase in the mass ratio, more wave modes are excited. As the frequencies of dominant modes become larger, the spectral range of the excited waves becomes broader. We can also find that the spectrum of magnetosonic waves changes from a discrete to a continuous spectrum with the increase of the mass ratio. These results are consistent with the growth rate profile obtained from the linear theory (red lines in Fig. 8). Figure 9(a) shows the energy of fluctuating magnetic field $\delta B^2/B_0^2$ versus the normalized wave frequency ω/Ω_h for case 5 and Figure 9(b) for case 2.

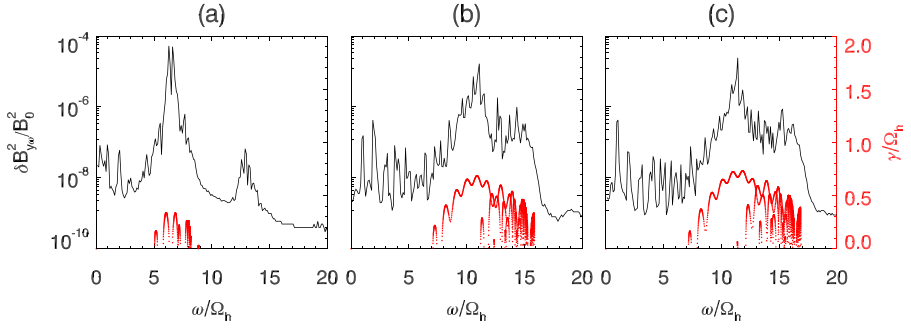

FIG. 8. The power spectrum obtained by Fourier transforming of $\delta B_y/B_0$ (black lines) from $\Omega_h t = 0$ to 60 for (a) case 3, (b) case 4, and (c) case 2. The red line in each panel denotes the growth rate γ/Ω_h calculated by the linear theory with the same parameters for the corresponding case.

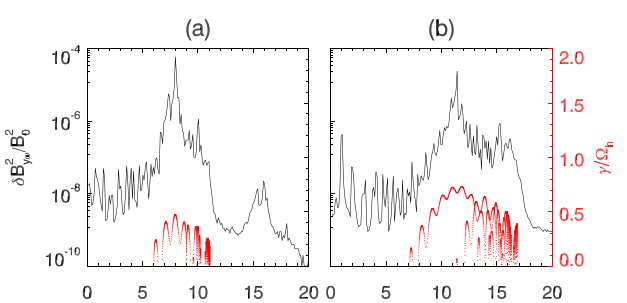

FIG. 9. The power spectrum obtained by Fourier transforming of $\delta B_y/B_0$ (black lines) from $\Omega_h t = 0$ to 60 for (a) case 5 and (b) case 2. The red line in each panel denotes the growth rate γ/Ω_h calculated by the linear theory with the same parameters for the corresponding case.

Similar to the increase of the mass ratio, the increase of the ratio of the light speed to Alfven speed favors the excited magnetosonic waves at larger frequencies and over a broader spectrum. The consistent linear theory results are displayed in Fig. 9 with the red lines, except the first few harmonics.

The effects of the number density of the ring distribution protons and the proton ring velocity on the spectrum of excited magnetosonic waves are also considered. With the increase of the number density or the velocity of the ring distribution protons, the dominant spectral range of the excited waves becomes broader (not shown).

IV. CONCLUSIONS AND DISCUSSION

In this paper, by performing 1D PIC simulations, we investigate the properties of the excited magnetosonic waves by a tenuous proton ring distribution under different plasma conditions, and the waves are assumed to propagate perpendicular to the background magnetic field. The spectrum of the excited magnetosonic waves may change from discrete to continuous if we increase the proton to electron mass ratio, the ratio of the light speed to the Alfven speed, or the concentration of protons with a ring distribution. When we increase the ring velocity of the tenuous proton ring distribution, the spectrum tends to change from a continuous one to a discrete one because the frequency range becomes broader with the unchanged free energy. These results are consistent with the prediction of the linear theory except for the first several harmonics. The formation of those low harmonics might be due to the proton ring distribution that experiences scattering by ion Bernstein waves. In addition, we also find that the excited magnetosonic waves can energize both cool electrons and protons preferentially in the perpendicular direction and scatter the ring distribution protons.

Satellite observations[9,10] have shown that magnetosonic waves in the inner magnetosphere usually have a discrete spectrum. However, recent observations have demonstrated that magnetosonic waves may also have a continuous spectrum. The results obtained in this paper provide valuable insight when one interprets different spectra of magnetosonic waves in the inner magnetosphere. According to our simulations, the energization of cool background plasma is very effective, which may enable them to become visible for the plasma instruments onboard various satellites in the inner Earth's magnetosphere.

ACKNOWLEDGMENTS

This research was supported by the National Science Foundation of China (Grant Nos. 41331067, 41474125, 11220101002, 11235009, 41174124, and 41121003), 973 Program (2013CBA01503 and 2012CB825602), and CAS Key Research Program (KZZD-EW-01-4).

[1]C. Russell, R. Holzer, and E. Smith, J. Geophys. Res. **75**, 755–768, doi:10.1029/JA075i004p00755 (1970).
[2]S. A. Boardsen, D. Gallagher, D. Gurnett, W. Peterson, and J. Green, J. Geophys. Res. **97**(A10), 14967–14976, doi:10.1029/92JA00827 (1992).
[3]O. Santolík, J. S. Pickett, D. A. Gurnett, M. Maksimovic, and N. Cornilleau-Wehrlin, J. Geophys. Res. **107**(A12), 1495, doi:10.1029/2001JA009159 (2002).
[4]O. Santolík, F. Nemec, K. Cereová, E. Macúsova, Y. de Conchy, and N. Cornilleau-Wehrlin, Ann. Geophys. **22**, 2587 (2004).
[5]Q. Ma, W. Li, R. M. Thorne, and V. Angelopoulos, Geophys. Res. Lett. **40**, 1895–1901, doi:10.1002/grl.50434 (2013).
[6]J. Sun, X. Gao, L. Chen, Q. Lu, X. Tao, and S. Wang, Phys. Plasmas **23**, 022901 (2016).
[7]K. Liu, S. P. Gary, and D. Winske, J. Geophys. Res. **116**, A07212, doi:10.1029/2010JA016372 (2011).
[8]L. Chen, R. M. Thorne, V. K. Jordanova, and R. B. Horne, J. Geophys. Res. **115**, A11222, doi:10.1029/2010JA015707 (2010).
[9]S. Perraut, A. Roux, P. Robert, R. Gendrin, J.-A. Sauvaud, J.-M. Bosqued, G. Kremser, and A. Korth, J. Geophys. Res. **87**(A8), 6219–6236, doi:10.1029/JA087iA08p06219 (1982).
[10]M. A. Balikhin, Y. Y. Shprits, S. N. Walker, L. Chen, N. Cornilleau-Wehrlin, I. Dandouras, O. Santolik, C. Carr, K. H. Yearby, and B. Weiss, Nat. Commun. **6**, 7703 (2015).